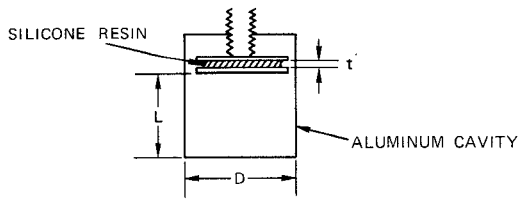

Fig. 1. Construction of tuning plunger for temperature compensation.

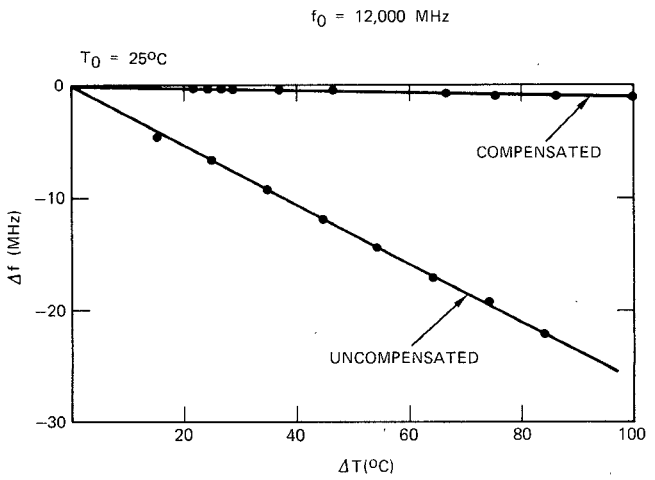

Fig. 2. Measured frequency shift with temperature of the compensated and uncompensated cavities.

Conclusions

A method for temperature compensation of TE_{011}-mode circular cavities is described and excellent frequency stability of a temperature-compensated aluminum cavity is demonstrated. These results should enable lightweight thermally stable bandpass filters to be constructed from aluminum instead of Invar and/or graphite-reinforced fibers. Significant savings in weight and cost of fabrication should therefore be achieved.

References

[1] *Techniques of Microwave Measurements*, C. G. Montgomery, Ed., Radiation Laboratory Series, vol. II. New York: McGraw-Hill, 1949.

Experimental Development of Simulated Biomaterials for Dosimetry Studies of Hazardous Microwave Radiation

AUGUSTINE Y. CHEUNG, MEMBER, IEEE, AND DAVID W. KOOPMAN

***Abstract*—Simulated biotissues have been developed which are appropriate for dosimetry studies at *X*-band frequencies and for *S*-band modeling experiments which would use miniature phantoms at *X*-band frequencies. A short-circuited waveguide system has been built and tested for the precise measurement of the dielectric properties of the simulated tissue. Modifications of composition for varying the dielectric properties over a wide range have been found. The specific heats of the materials have been measured and are approximately the same as the tissues they represent.**

Manuscript received January 28, 1976; revised April 15, 1976. This project was supported by the Division of Electronic Products, U.S. Bureau of Radiological Health, Rockville, MD, under Contract FDA-7417.

A. Y. Cheung is with the Department of Radiology, Section of Radiation Physics and Radiation Biology, University of Maryland at Baltimore and the Institute for Fluid Dynamics and Applied Mathematics, University of Maryland, College Park, MD 20742.

D. W. Koopman is with the Institute for Fluid Dynamics and Applied Mathematics, University of Maryland, College Park, MD 20742.

I. Introduction

The increasing use of microwaves in radar, ovens, high-frequency communications systems, and new medical and industrial devices has subjected the human population to appreciable levels of short-wavelength electromagnetic radiation. Biological effects of microwave radiation have been reported on many occasions but there is still much uncertainty about the hazards stemming from exposure and the mechanisms, thermal or nonthermal, responsible for the observed effects.

Most analyses on microwave field-related hazards are based on a plane-wave approximation, which may be valid only for far-field regions. However, most hazardous exposure often occurs in the near-field zone, where the field lines may be curved and exhibit strong power gradients. In this region, the human body may interact with and modify the incident radiation field [1]. Unlike ionizing radiation, which travels in essentially straight paths within the body, microwave radiation is modified by reflection, refraction, and diffraction effects, due to the geometrically varying dielectric and absorption properties of tissues. As a result, theoretical analysis of microwave dosimetry is a complicated problem and it is difficult to relate external radiation-field strengths to the actual power density within the body. An alternate approach to quantify hazardous fields is to perform experimental measurements inside artificial tissues or phantom materials which simulate the electrical properties, specific heat, and the size and shape of a human. Guy has developed materials simulating human tissues at *S*-band frequencies ($f \sim 2450$ MHz) [2]. In order to set a wide-band safety exposure standard, measurements must also be made in other frequency ranges, specifically the higher *X* band ($f \sim 9$ GHz) which is widely used in radar systems.

II. Scientific Objectives

One goal of our research has been to develop phantom materials which have a range of dielectric properties and specific heat similar to those of tissues within the human body in the *X*-band frequency range at 20°C. We studied the influence of composition on properties at frequencies of 8.5 and 10.0 GHz for two types of materials, one corresponding to tissues of high water content (muscle) and the other for bone and fatty layers. Table I summarizes the dielectric properties of human tissue at *X*- and *S*-band frequencies as reported by Schwan at 37°C [3].

In addition to developing artificial tissue for *X*-band studies, it is also our goal to simulate *S*-band total body radiation using smaller and more convenient scale-model phantoms at *X*-band frequencies. If the model is to be reduced in size from the full scale by a linear factor *S*, then it can be shown that electromagnetic scaling is achieved if [4]

$$\omega_m = S\omega$$

$$\mu_m = \mu$$

$$\varepsilon_{r_m}' = \varepsilon_r'$$

$$\tan \delta_m = \tan \delta \quad \text{or} \quad \sigma_m = S\sigma$$

with the subscript m denoting the model.

Examination of Table I shows that the materials needed for the scaling of quarter-sized models to simulate *S*-band exposure by *X*-band measurements are not greatly different from phantom materials required for full-scale *X*-band studies. In attempting to produce suitable phantom materials, we employed materials based on the previous work of Guy [2], which had been successful for making *S*-band phantoms at 20°C, and varied the composition to obtain the desired *X*-band properties. Muscle is

TABLE I
DIELECTRIC PROPERTIES OF HUMAN TISSUE AT 37°C

	S-BAND(3.0 GHz)			X-BAND(8.5 GHz)			
	Dielectric Constant ϵ'_r	Loss Tangent tan δ	Conductivity (Millimhos/cm) σ	Dielectric Constant ϵ'_r	Loss Tangent tan δ	Conductivity (Millimhos/cm σ	Specific Heat
MUSCLE	45-48	.27-.31	21-23	40-42	.35-.37	83	.84
BRAIN	34	.27	15.3	-	-	-	.83
BONE & FAT	4-7	.17-.55	1-2.3	3.5-4.5	.15-.25	2.7-4.2	.29-.37

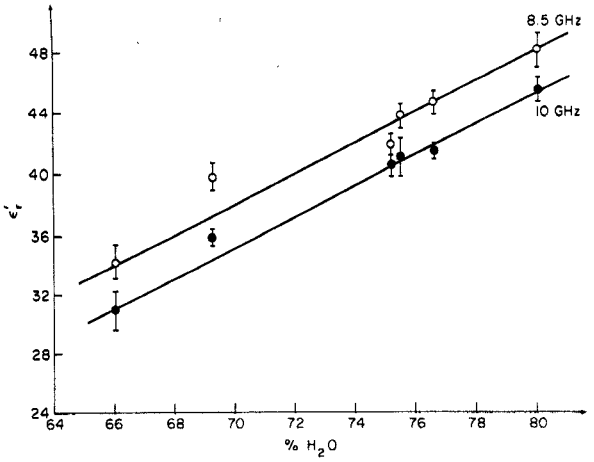

Fig. 1. Schematic arrangements of short-circuited waveguide system for dielectric measurement.

simulated by a gelling plastic Super Stuff (Whamo Manufacturing), water, polyethylene powder, and sodium chloride; simulated bone consists of Laminac 4110 (a polyester resin), acetylene black, and aluminum powder.

III. Techniques of Measurement

Various methods of dielectric measurements were examined and the short-circuit waveguide technique was chosen [5]. A schematic diagram of the measurement system is shown in Fig. 1. The microwave source is a Hewlett-Packard 8620B sweeper with a 86250A RF plug-in. The operating frequency is continuously monitored by a crystal detector connected to an absorption wavemeter (HP X 532 B), isolated from the rest of the system by means of a 20-dB directional coupler. In order to avoid unwanted reflection due to impedance mismatches, isolators are used throughout the system whenever there is a discontinuity. The input power level to the system is always adjusted to 10 mW using a variable attenuator and further variation of signal level during a measurement can be achieved by a precision attenuator. A slide-screw tuner is also used to maximize the signal level available to the slotted-line detector.

The slotted section consists of a PRD 230 probe carriage and a 250-A tunable crystal detector. In this experiment, the width of the standing-wave node is measured instead of using a VSWR meter for direct measurement to avoid error introduced by nonlinearity of the meter. The node widths, both with and without the sample, are measured. Due to the sharpness in the standing-wave pattern in the absence of the sample, the 10-dB width is measured instead of the conventional 3-dB width, which is used when the sample is present.

Solid-plastic simulated bone samples are cast inside a waveguide and milled to lengths determined with an accuracy within 0.02 mm. The jellied plastic muscles are packed into the sample holder by an aluminum plunger machined to fit snugly inside the waveguide and a scale is set on the plunger which measures the thickness of the sample correctly to 0.1 mm.

To measure the node width, a voltage minimum is first located and after noting the voltmeter reading at the minimum, the power level is attenuated to a level between 3 and 10 dB by the precision attenuator. The probe is then moved to both sides of the minimum and the positions of the probe at which the power level returns to the original minimum level are recorded. The difference between the vernier reading on each side is recorded as the node width. The desired quantities are then computed from the frequency, sample length, air node and sample node position, air node and sample node decibel level and width, and the dimensions of the waveguide [6]. Corrections for the influence of the slot and wall losses in the waveguide, as well as the difference between air and a true vacuum, have also been included.

IV. Results and Analysis

Samples corresponding to various compositions of simulated bone and muscle plastic mixtures were analyzed. At 20°C for each composition, many samples with thickness ranging from 2 to 15 mm were used. Our results indicate that for the low-dielectric-constant, low-loss samples (bone, solid plastic), measurements were consistent regardless of the sample length. However, for high-dielectric-constant, high-loss samples (muscle), only sample lengths centered around $l \simeq (n + 1/4)\lambda_0/\sqrt{\varepsilon_r}$ can generate accurate results [7].

Measurements were made on muscle mixtures *A–F* and bone mixtures *A–I* (see Table II for their composition), selecting sample lengths so that they all fall within neighborhoods of the sensitive region ($\sim 1.25\lambda$ for muscles, in our case). For each mixture, many values of ε_r' and σ (or tan δ) were obtained so that a mean and a standard deviation together specify each dielectric parameter of a given mixture. Specific heat measurements using standard calorimetric techniques were also made on each sample. The dielectric and heat properties of the simulated materials are tabulated in Tables II and III.

V. Composition Analysis and Materials Selection

With the bone materials, which are simulated by a mixture of Laminac 4110, aluminum powder, and acetylene black (see [2] for detailed information about supplies and mixing techniques), it is difficult to describe the dielectric properties as a function of composition. All components contribute significantly to the dielectric constant and loss tangent and no distinction between

TABLE II
COMPOSITION AND DIELECTRIC PROPERTIES OF SIMULATED MUSCLES AT 20°C

	Composition					Properties				
	% Super Stuff	% Poly-Ethylene	% Water (H_2O)	% Salt (NaCl)	Molarity (NaCl-H_2O)	f (GHz)	Dielectric Constant ϵ_r'	Loss Tangent $\tan\delta$	Conductivity (Millimhos/cm) σ	Specific Heat
A	8.45	15.20	75.44	.9069	.2055	8.5	43.63 ± .82	.3208 + .0190	63.84 ± 3.73	.844
						10.0	40.90 ± 1.32	.3206 ± .0330	66.88 ± 7.17	
B	8.45	14.00	76.55	1.0000	.2233	8.5	44.42 ± .77	.3101 ± .0175	62.71 ± 3.68	.878
						10.0	41.17 ± .41	.3281 ± .0213	72.13 ± 4.71	
C	8.45	15.20	75.15	1.2000	.2730	8.5	41.29 ± .91	.3050 ± .0252	56.70 ± 4.14	.885
						10.0	40.47 ± .68	.2945 ± .0246	62.18 ± 5.34	
D	7.50	25.00	66.00	1.5000	.3885	8.5	34.31 ± 1.18	.3539 ± .0294	53.65 ± 6.20	.763
						10.0	30.94 ± 1.35	.3665 ± .0305	60.55 + 4.09	
E	8.00	22.50	69.20	.3000	.0741	8.5	39.92 ± .82	.2380 ± .0461	37.49 ± 8.33	.625
						10.0	35.75 ± .48	.2924 ± .0225	53.32 ± 5.02	
G	9.00	9.50	80.00	1.5000	.3205	8.5	47.80 ± 1.20	.3067 ± .0318	66.30 ± 5.45	.880
						10.0	45.28 ± .88	.3289 ± .0116	82.63 ± 1.92	

TABLE III
COMPOSITION AND DIELECTRIC PROPERTIES OF SIMULATED BONE AND FATTY TISSUES AT 20°C

	Composition						Properties				
	Laminac 4110		Aluminum Powder		Acetylene Black		f (GHz)	Dielectric Constant ϵ_r'	Loss Tangent	Conductivity (Millimhos/(cm))	Specific Heat
	% Wt	% Vol	% Wt	% Vol	% Wt	% Vol			$\tan\delta$	σ	
A	85.20	89.61	14.50	10.17	.24	.23	8.5	3.99 ± .03	.0770 ± .0039	1.42 ± .09	.308
							10.0	3.98 ± .03	.0688 ± .0022	1.52 ± .05	
B	87.20	91.07	12.50	8.70	.24	.23	8.5	3.83 ± .04	.0812 ± .0022	1.46 ± .04	.290
							10.0	3.83 ± .05	.0973 ± .0083	1.98 ± .14	
C	81.25	86.88	18.00	12.83	.30	.29	8.5	5.18 ± .05	.1533 ± .0085	3.70 ± .22	.352
							10.0	4.67 ± .09	.1509 ± .0162	3.76 ± .29	
D	74.05	81.22	25.00	18.28	.50	.49	8.5	5.98 ± .10	.1801 ± .0042	5.08 ± .17	.270
							10.0	5.66 ± .17	.2271 ± .0236	6.92 ± .57	
E	84.55	89.31	14.50	10.21	.50	.48	8.5	4.26 ± .08	.1385 ± .0043	2.76 ± .15	.293
							10.0	4.07 ± .03	.1410 ± .0065	3.16 ± .83	
F	83.95	88.85	15.00	10.58	.60	.57	8.5	4.72 ± .04	.1675 ± .0049	3.73 ± .11	.289
							10.0	4.60 ± .07	.1663 ± .0075	4.21 ± .19	
G	80.80	86.44	18.00	12.84	.75	.72	8.5	5.34 ± .06	.2083 ± .0047	5.24 ± .17	.293
							10.0	5.08 ± .09	.2028 ± .0084	5.68 ± .21	
H	73.85	81.02	25.00	18.29	.70	.69	8.5	5.96 ± .09	.1903 ± .0182	5.19 ± .35	.292
							10.0	5.72 ± .10	.1843 ± .0199	5.54 ± .49	
I	83.65	88.67	15.50	10.95	.40	.38	8.5	4.54 ± .08	.1343 ± .0009	2.88 ± .04	.298
							10.0	4.38 ± .05	.1233 ± .0070	2.95 ± .17	

dominant and perturbation component can be made. However, from the tabulated results in Table III, it is possible to obtain a rough estimate based on a general trend exhibited by the measured samples. It has been confirmed experimentally that estimated compositions to produce a desired characteristic over ranges prescribed by bones *A–I* are correct to within 10 percent.

The dielectric properties of muscle can basically be described as a function of the major contributing component, water. From a graph of ε_r' versus $\%H_2O$, we find a linear relation (Fig. 2). In fact [8]

$$\varepsilon_r' \simeq 5 + (70\text{-}P)/[1 + (1.5/\lambda_0)^2]$$

where

λ_0 free-space wavelength;
P volume fraction of nonaqueous components.

Using P approximately equal to the weight fraction since the specific gravity of the samples are very close to unity, we have, at 20°C

$$\varepsilon_r' \simeq (\%H_2O - 30)[1 + (f/20)^2]^{-1} + 5$$

where f is in gigahertz. Our measured values and the calculated values from this theory are in excellent agreement (see Table IV).

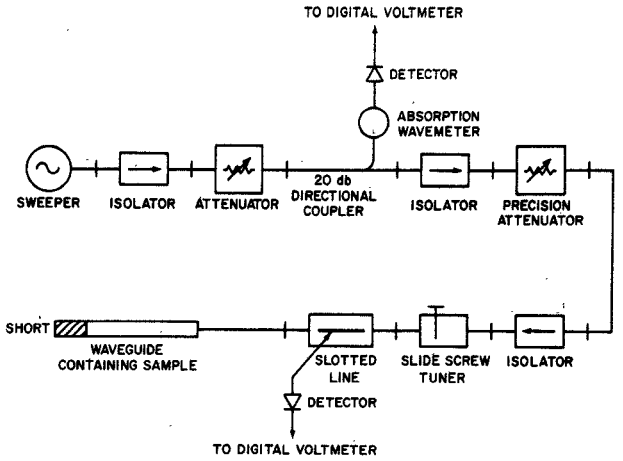

Fig. 2. Relative dielectric constants (ε_r') of simulated muscles versus percentage of water at 8.5 and 10.0 GHz at 20°C.

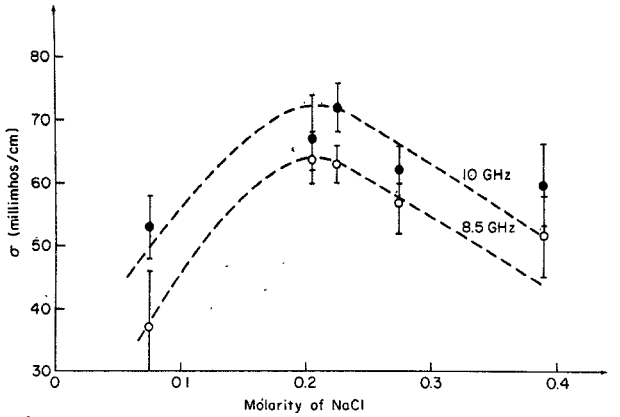

Fig. 3. Measured conductivity of simulated muscle versus molarity of salt at 8.5 and 10.0 GHz at 20°C.

TABLE IV
COMPARISON BETWEEN MEASURED AND CALCULATED VALUES OF DIELECTRIC CONSTANT ε_r' OF SIMULATED MUSCLES

	8.5 GHz		10.0 GHz	
Muscle	Measured	Calculated	Measured	Calculated
A	43.63 ± .82	43.49	40.90 ± 1.32	41.35
B	44.42 ± .76	44.43	41.17 ± .41	42.24
C	41.29 ± .91	43.24	40.47 ± .68	41.12
D	34.31 ± 1.18	35.49	30.94 ± 1.35	33.80
E	39.92 ± .82	38.20	35.75 ± .48	36.36
G	47.80 ± 1.20	47.35	45.28 ± .88	45.00

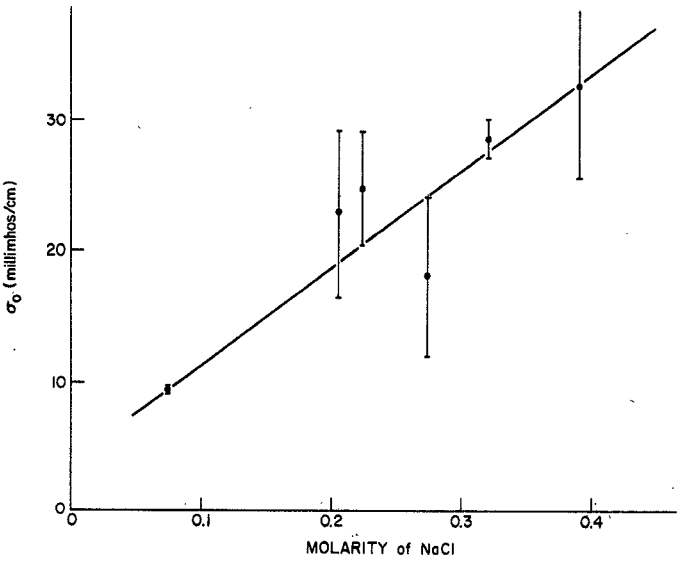

Fig. 4. Static conductivity (σ_0) of simulated muscles versus molarity of salt at 20°C.

The conductivity σ, of the mixtures was first thought to be dominated by the salt content. However, as demonstrated by Fig. 3, our measured values did not show a simple relation between σ and the molarity of the salt solution. We found the conductivity at microwave frequencies is due to the frequency-dependent dispersion characteristics of water as well as the low-frequency component due to the salt content. The conductivity relationship at 20°C is expressed by [8]

$$\sigma = \sigma_0 = (\%H_2O - 30)(f^3/7.2 \times 10^5)[1 + (f/20)^2]^{-1}$$

where

σ_0 low-frequency conductivity due to salt content at 20°C.

From our measured values of σ at the two frequencies σ_0 can be calculated for each mixture composition. We find indeed that σ_0 is a linear function of the salt molarity, as shown in Fig. 4, and that $(\sigma - \sigma_0)$ is linearly proportional to the percentage of water, as shown in Fig. 5.

CONCLUSION

Based on the measured dielectric properties, muscle (A) and bone (E) have been chosen for X-band studies; and muscle (F) and bone (G) will be used for the S-band modeling experiments.

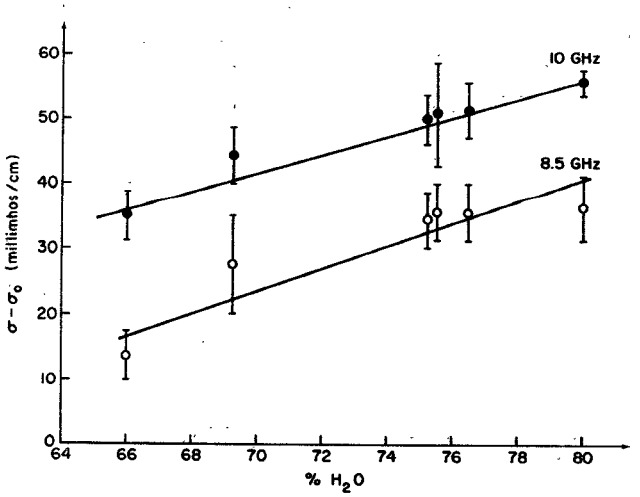

Fig. 5. High-frequency conductivity of simulated muscle versus percentage of water at 20°C.

The procedures for precision dielectric and loss measurements have been developed as described, allowing the construction of the two groups of simulated biotissues. The formulations for the properties of high-water-content materials are valuable for finding phantom materials for many parts of the human body which have a wide range of dielectric properties.

Acknowledgment

The authors wish to thank J. Saffer for performing the measurements and data analysis. The discussions with Mr. Swicord and Dr. Ho of the Bureau of Radiological Health have been extremely useful. They also wish to thank Dr. S. Nelson for supplying his computer program for dielectric-measurement data analysis, and H. Levene for preparing the samples.

References

[1] P. F. Wacker and R. R. Bowman, "Quantifying hazardous electromagnetic fields: Scientific basis and practical considerations," *IEEE Microwave Theory Tech.*, vol. MTT-19, no. 2, 1971.
[2] A. W. Guy, "Analyses of electromagnetic fields induced in biological tissues by thermographic studies on equivalent phantom models," *IEEE Microwave Theory Tech.*, vol. MTT-19, no. 2, 1971.
[3] H. P. Schwan, "Radiation biology, medical applications, and radiation hazards," *Microwave Power Engineering*, vol. 2, E. C. Okress, Ed. New York: Academic Press, 1968, pp. 215–232.
[4] W. L. Weeks, *Electromagnetic Theory for Engineering Applications*. New York: John Wiley, 1964, pp. 46–48.
[5] A. R. Von-Hippel and S. Roberts, "A new method for measuring dielectric constants and loss in the range of centimeter waves," *J. Appl. Phys.*, vol. 17, no. 7, 1946.
[6] S. O. Nelson, C. W. Schlaphoff, and L. E. Stetson, "Computation of dielectric properties from short-circuited waveguide measurements on high or low-loss materials," *IEEE Microwave Theory Tech.*, vol. MTT-22, no. 3, 1974.
[7] A. R. Von-Hippel, *Dielectrical Materials and Applications*. New York: John Wiley, 1954, pp. 75–80.
[8] H. P. Schwan, "Interaction of microwave and radio frequency radiation with biological systems," *IEEE Microwave Theory Tech.*, vol. MTT-19, no. 2, 1971.

Observation and Application of High-Order Azimuthal Modes in a Fabry–Perot Resonator

CLIFFORD W. ERICKSON

Abstract—**High-order azimuthal modes ($p = 0, l > 20$) were excited at 10 GHz in a Fabry–Perot resonator. The energy of these modes is distributed in a ring around an energy-free central axis, which lends itself to safety applications on rotating machinery and in measuring density profiles of cylindrical plasmas.**

Introduction

High-order modes in Fabry–Perot resonators have been reported both at laser and at microwave frequencies [1], [2]. Generally, the higher the mode order the greater the radial extent of the beam on the mirror, and therefore a higher energy loss, so that in conventional applications of lasers and beam waveguides these modes are considered undesirable. In this short paper we report on high-order azimuthal modes observed at 10 GHz and describe a device which is based on such high-order modes.

Manuscript received December 22, 1975; revised April 19, 1976.
The author is with the Honeywell Corporate Research Center, Bloomington, MN 55420.

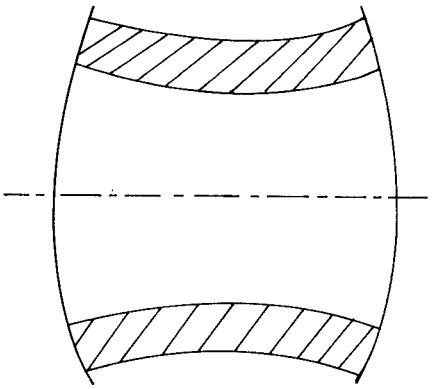

Fig. 1. Cross-sectional representation of the energy distribution of $l = 25$ mode in the $\phi = 0$–$180°$ plane. Boundaries of the shaded area are contours of constant intensity equal to e^{-2} times the peak value in the midplane.

Theory

In the large aperture approximation [1] the amplitude of a component of the electric field is given as (cylindrical coordinates r, z, ϕ)

$$\psi_p^{\,l} = \left(\sqrt{2}\,\frac{r}{w}\right)^l L_p^{\,l}\left(\frac{2r^2}{w^2}\right)\frac{w_0}{w}\exp\left(-r^2/w^2\right)\cos l\phi \cdot \exp\left\{j\left[(2p + l + 1)\tan^{-1} az - r^2/w^2 az\right]\right\} \quad (1)$$

where p and l are the radial and azimuthal mode numbers, respectively, and the remaining parameters are defined as follows:

w_0^2 $(\lambda/2\pi)[d(2R - d)]^{1/2}$;
d spacing between mirrors;
R radius of curvature of the mirrors;
a $\lambda/\pi w_0^2$;
w $w_0[1 + a^2z^2]^{1/2}$.

If p is restricted to zero the expression in (1) is simplified such that in the midplane of the device the intensity of the field is

$$(\psi_0^{\,l})^2 = (2r^2/w_0^2)^l \exp\left(-2r^2/w_0^2\right)\cos^2 l\phi. \quad (2)$$

This function is zero on the axis of the resonator and has $2l$ maxima on a radius $r_{max} = w_0\sqrt{l/2}$. The circumference implied by this radius is just $2\pi w_0\sqrt{l/2}$, so that the distance between adjacent azimuthal maxima is just $\pi w_0/\sqrt{2l}$.

Thus, the higher the value of l the larger the area near the axis which is free of energy and the closer to each other are the adjacent azimuthal maxima. Fig. 1 shows a cross section of energy in the $\phi = 0$–$180°$ plane for $l = 25$.

Experiment

We have excited such modes at X band with l as high as 25. Distribution of mode energy was measured with the absorptive probe method described in [2]. The value of l was determined by using as a probe a thin ceramic rod rigidly fixed perpendicular to a larger shaft on the axis of the device. Each revolution of the shaft swept the ceramic rod through $2l$ maxima.

The mirrors were identical to those in [2], with the exception that the azimuthal modes were excited through coupling irises near the edge of the mirror rather than on the axis. A three-dimensional oscilloscope representation of the energy distribution in the midplane of the device is shown in Fig. 2. Note that with an l of 25 the adjacent maxima are so close together that they are just able to be distinguished in those places on the